대한조선학회논문집
Journal of the Society of Naval Architects of Korea
Vol. 48, No. 6, pp. 581-591, December 2011
http://dx.doi.org/10.3744/SNAK.2011.48.6.581

CFD 기반 유체충격 해석에서 공기 압축성 효과

찬후피[1] · 안형택[2,†]
Baker Hughes Inc.[1]
울산대학교 조선해양공학부[2]

Air Compressibility Effect in CFD-based Water Impact Analysis

Tran Huu Phi[1] · Hyung Taek Ahn[2,†]
Baker Hughes Inc.[1]
School of Naval Architecture and Ocean Engineering, University of Ulsan[2]

Abstract

This paper describes the air compressibility effect in the CFD simulation of water impact load prediction. In order to consider the air compressibility effect, two sets of governing equations are employed, namely the incompressible Navier-stokes equations and compressible Navier-Stokes equations that describe general compressible gas flow. In order to describe violent motion of free surface, volume-of-fluid method is utilized. The role of air compressibility is presented by the comparative study of water impact load obtained from two different air models, i.e. the compressible and incompressible air. For both cases, water is considered as incompressible media. Compressible air model shows oscillatory behavior of pressure on the solid surface that may attribute to the air-cushion effect. Incompressible air model showed no such oscillatory behavior in the pressure history. This study also showed that the CFD simulation can capture the formation of air pockets enclosed by water and solid surface, which may be the location where the air compressibility effect is dominant.

Keywords : Water Impact(유체충격), Air Compressibility(공기압축성), Navier-Stokes equations(나비어-스톡스방정식), Computational Fluid Dynamics(CFD,전산유체역학), Volume-of-fluid(VOF, 유체체적법)

1. Introduction

Hydrodynamics of free-surface flows that causes impact loads on the marine structures has not been fully understood. Prediction of the impact loads is essential in designing ships and offshore structures. Green water on ship deck, wave run-up on offshore structures, slamming and sloshing in tank are among the representative examples of water impact phenomena in the area of naval hydrodynamics (Wu et al. 2004, Howison et al. 2001, Sun and Faltinsen 2006). Available theories such as potential theory (Korobkin and Iafrati 2005, Wu 1998), which is commonly solved by a boundary element method (BEM) (Wu et al. 2004, Zhao and Faltinsen 1993, Sun and Faltinsen 2006), showed limited success on water problems involving violent free surface deformation. Perhaps, this is because, in addition to the free-surface geometrical complexities, discontinuities in the flow and air entrainment and compressibility effects in these problems are difficult to be treated satisfactorily.

New trends are towards direct numerical solutions of Navier-Stokes equations (Yum and Yoon 2008, Lee et al. 2008, Kleefsman et al. 2005, Zhang et al. 2010). Yoon (1991) and Lee et al. (2008) applied Lagrangian and particle based methods for water impact simulation. Kang and Troesch (1990) reported impact load prediction for 3D bodies. More recently, Nho et al.(2010) reported structural response due to the water impact load.

In this endeavor, it is necessary to find a proper mathematical model (the governing equations) that best describes the complex water impact problem. Different numerical techniques and methods are under investigation to explore complex free-surface and impact problems. Among the large volume of literature written on this subject, Scardovelli and Zaleski (1999) provides a good review and highlights the problems associated with numerical techniques.

Most of the previous study on water impact assumes the fluid as incompressible media (Yum and Yoon 2008, Lee et al. 2008) and few work has been done about compressible fluids (Godderidge et al. 2009). However, when water impacts on flat surface, like ship with wide flat bottom, water slamming

접수일 : 2010년 8월 31일 | 1차 수정일 : 2011년 1월 9일 | 게재확정일 : 2011년 8월 29일
†교신저자 : htahn@ulsan.ac.kr, 052-259-2164

often involves air trapping and air cushion effect. A pioneering experimental work of flat bottom water slamming is being carried out by Kwon et al. (2010). In this case, the compressibility effects of air may play an important role and its effect is not clearly reported. A new computational research for better understanding of water impact and air compressibility associated with it is also desired.

In this study, air is considered both compressible and incompressible media by employing compressible Navier-Stokes equations for ideal gas and incompressible Navier-Stokes equations for incompressible air model respectively. Volume-of-fluid (VOF) method is used to describe deformation of free surface. In order to save time and effort related to the development and verification of two different sets of flow solvers (compressible and incompressible Navier-Stokes solvers), a general purpose CFD package, Fluent (2008), is utilized.

The effect of air compressibility is investigated by the comparison of compressible and incompressible simulations. The results are presented in impact pressure on the solid surface, forces acting on the solid surface, and impulse exerted during the impact process. Also, the effect of air compressibility with respected to different domain sizes is investigated.

This paper is organized as follows. In Sec. 2, the governing equations for both compressible and incompressible flows are presented. For the free surface representation, the basic concept of Volume-of-Fluid method is introduced. In order to check the validity of current compressible air model, a simple compression test involving evolving free surface is presented in Sec. 3. The role of air compressibility is presented in Sec. 4 by considering water drop impact on the flat solid surface. Histories of pressure, force, impulses are compared for compressible and incompressible models. Time step refinement and mesh refinement study is presented for the convergence check. Scale effect is also discussed with a series of simulations with different domain size. This paper is summarized in the following conclusion section.

2. Governing Equations

In this section we present two sets of governing equations, namely compressible and incompressible Navier-Stokes equations. For the representation of free surface evolution, volume-of-fluid (VOF) method is employed and its basic concept is presented.

2.1 Compressible Navier-Stokes Equations

In order to consider the compressibility of the air, we consider the compressible Navier-Stokes equations. The compressible Navier-Stokes equations consisted of continuity, momentum, and energy equations can be expressed as follows in differential form.

$$\frac{\partial}{\partial t}(\rho)+\nabla\cdot(\rho V)=0 \tag{1}$$

$$\frac{\partial}{\partial t}(\rho V)+\nabla\cdot(\rho VV)=V\cdot(T)+\rho f \tag{2}$$

Here ρ is the density of the fluid, V is the fluid velocity, f is the body force per unit mass, T is the stress tensor whose components are expressed as follows,

$$(T)_{ij}=-p\delta_{ij}+\mu\left(\frac{\partial u_i}{\partial x_j}+\frac{\partial u_j}{\partial_i}\right)+\delta_{ij}\lambda\frac{\partial u_k}{\partial x_k}$$

where p is the pressure, μ is the viscosity, and λ is the second coefficient of viscosity.

$$\frac{\partial}{\partial t}(E)+\nabla\cdot(EV)=\nabla\cdot(T\cdot V)-\nabla\cdot(q)+\rho f\cdot V \tag{3}$$

For the energy equation as shown in Eq. (3), E is the total energy per unit volume and q is the heat flux.

The system of compressible Navier-Stokes equations is composed of $N_{sd}+2$ equations, where N_{sd} is the number of spatial dimensions. Whereas the unknowns appearing in the system are p, ρ, e, T, and u_j, the velocity components, i.e. total $N_{sd}+4$ unknowns. Hence, two auxiliary equations are necessary for the system of equations to be closed.

$$p=p(\rho,T),e=e(\rho,T)$$

The above two equation are general representation of thermal and caloric equations of state, respectively. For ideal and calorically perfect gas (gas at relatively low temperature) the above equations can be expressed as follows:

$$p=\rho RT,\ e=c_vT$$

where c_v is the specific heat at constant volume.

2.2 Incompressible Navier-Stokes Equations

The flow can be considered as incompressible in case the density variation is negligible regardless of pressure. Typically low speed air flow and most of water flow can be considered as incompressible. Once the flow is assumed as incompressible, then the density is constant, and the original compressible

Navier-stokes equations can be simplified as follows,

$$\nabla \cdot V = 0 \tag{4}$$

$$\rho\left(\frac{\partial}{\partial t}V + V \cdot \nabla V\right) = \nabla \cdot (-pI + \tau) + \rho f \tag{5}$$

where τ is the viscous stress tensor and its component is defined as follows,

$$(\tau)_{ij} = \mu\left(\frac{\partial u_i}{\partial x_j} + \frac{\partial u_j}{\partial x_i}\right)$$

The above system of equations composed of continuity and momentum equation involves unknowns of and velocity components. The incompressible Navier-Stokes equations are now closed to be solved.

2.3 Volume-of-fluid Method

In order to represent dynamically evolving free surface, we employ Volume-of-Fluid method. The volume of fluid (VOF) method is a numerical technique for tracking and locating the free surface or fluid-fluid interface. It belongs to the class of Eulerian methods that represents the moving interface based on volume-fraction information being updated at each time.

The method is based on the idea of so called volume fraction function f. It is defined as the integral of fluid's characteristic function in the control volume. Basically, if the cell is empty (there is no traced fluid inside) $f = 0$, if the cell is full, we have $f = 1$, and if the interface cuts the cell, then $0 < f < 1$.

The fraction function f is a scalar function and convected passively by the fluid velocity. The evolution equation of the volume fraction f can be represented simply by an advection equation described as follows,

$$\frac{Df}{Dt} = \frac{\partial}{\partial t}f + V \cdot \nabla f = 0 \tag{6}$$

Based on the volume fraction at each computational cell, interface between the air and water is represented by the Piecewise-Linear Interface Calculation (PLIC) scheme.

3. Simple Compression Test

3.1 Problem Definition

The purpose of this test is to validate compressible air model governed by compressible Navier-Stokes equations. A schematic diagram of the simple compression test model is presented in Fig. 1.

In this test, the tank size is 0.1 m in width, 1 m in height and the lower half of this tank is filled with water at the initial configuration, i. e. the water column has a initial height of 0.5 m. Now, the water column is set to move upward with constant velocity of 0.001 m/s by the imposition of the bottom boundary as a velocity inlet.

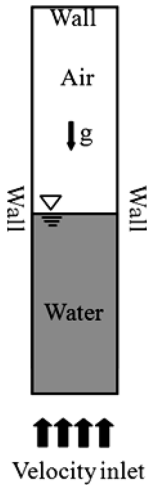

Fig. 1 General layout of the compression test

Water is considered as viscous fluid with a constant density. Air is considered as ideal gas with a reference temperature of 298.15(K). The flow is modeled as laminar. The left wall, right wall and top wall are treated as a stationary wall with no slip condition. In this compression test, two different wall boundary condition is applied for the energy equations, namely isothermal (constant temperature) and adiabatic (no heat flux) wall boundary conditions.

3.2 Results

The rectangular domain is discretized by using quadrilateral cells. The grid size of 100×100 and the time step size of 0.05 second were employed. The result of this simple compression is displayed in Fig. 2 for adiabatic wall and Fig. 5. for isothermal wall boundary conditions.

In the adiabatic compressibility model, as shown in Fig. 2, there is a noticeable deviation of pressure-density relationship from the ideal gas low especially at the beginning of the compression. This deviation is caused by the temperature increase of air phase due to the adiabatic compression. As the compression progresses heat exchange between the air and water phase decrease the air temperature as shown in

Fig. 3. Overall the pressure density relationship follows the ideal gad law well except at the initial stage of air temperature increase.

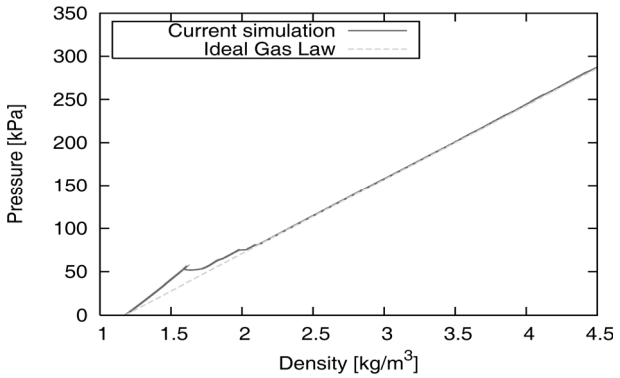

Fig. 2 Pressure-density relation of the compressible air during the simple compression test-adiabatic wall boundary

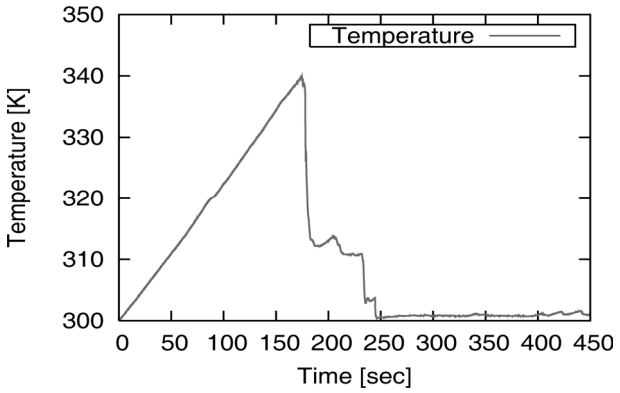

Fig. 3 Temperature history of the compressible air during the simple compression test-adiabatic wall boundary

In the isothermal compressibility model, the wall temperature is fixed to the initial air temperature. Hence, the air temperature is kept almost constant though the entire compression progresses. This is shown in Fig. 5. It is also confirmed that

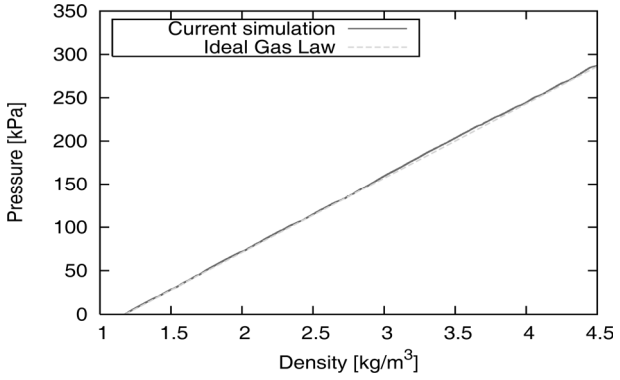

Fig. 4 Pressure-density relation of the air phase with the isothermal compressibility model

with constant air temperature, the pressure-density relation follows perfectly the one obtained by the ideal gas law as shown in Fig. 4. This result strengthens the validity of the current compressible air modeling.

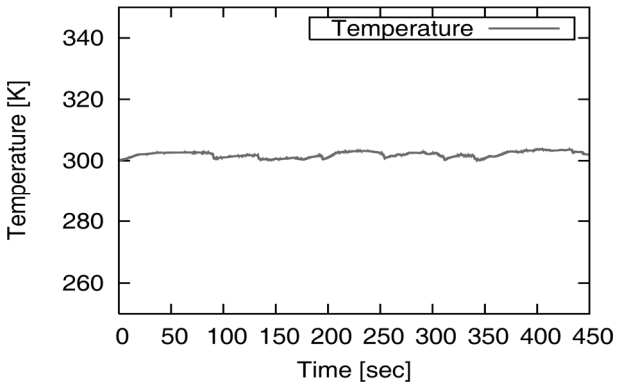

Fig. 5 Temperature history of the air phase with the isothermal compressibility model

Fig. 6 shows snapshots of the air/water interface evolution at different time moments. For the result the adiabatic wall boundary condition is used. Slight asymmetricity in the interface can be attributed to the non-linear nature of the Navier-Stokes equations.

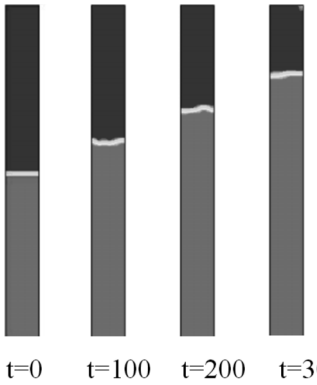

Fig. 6 Water phase evolution with the adiabatic compressibility model. Red-water, blue-air

4. Water Drop Problem

4.1 Problem Definition

The water impact problem modeled in this study is illustrated in Fig. 7. In this model, the tank size is L=1 m and H=1 m. Initially, a block of water (L=0.4 m and H=0.4 m) is located at the center of the tank. For impact pressure measurements on the bottom wall, a sensor point P0(0.5 m, 0 m) is located at the center of the bottom.

Water is considered as viscous fluid with a constant density. Flow is considered as laminar and no turbulence model is employed. Since the major interest of current study is about water impact force, which is an inertia-dominated force, no effect of turbulence is encountered although further investigation about the effect of turbulence is strongly encouraged. Air is considered in two different models: constant density incompressible air and compressible air following ideal gas law as validated in the previous section. The flow is modeled as laminar.

As shown in Fig. 7, the boundary conditions are all set as adiabatic no-slip wall conditions except for the tank top, which is set as pressure outlet. The pressure outlet boundary condition maintains a zero gauge pressure (same as the atmospheric pressure) at the defined boundary, which is desired for the tank top. The falling of the fresh water block, initially at rest, is initiated by the gravitational acceleration.

The size of time step plays an important role in unsteady simulation of fluid flow. We present time step refinement study for two different levels of meshes to check if the solution converges as the time step refines. Three levels of successively refined time steps were used to examine its effects to the results.

A proper time step, which provides converged results, is a function of grid size applied to the problem. For the case A1: 100×100 mesh, considering $\triangle t = 0.001\mathrm{sec}$ and the approximate impact velocity $V_{impact} = \sqrt{2gH} = 2.426\,m/s$, the maximum value of Courant number over the domain can be approximated as $CFL = \frac{V_{impact}\triangle t}{\triangle x} = 0.243$. The initial time step for the time step refinement study is determined based on the previous computation so that the maximum Courant number near the free surface does not violate the CFL stability condition. The Courant number for this test was set to 0.25.

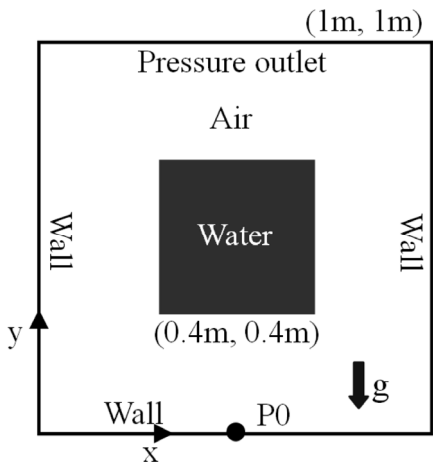

Fig. 7 General layout of the water drop test

4.2 Results

4.2.1 Compressible Air

In order to see the effect of air compressibility, the air is considered as compressible ideal gas. The time histories of pressure and vertical force acting on the bottom surface are shown in Fig. 8 and Fig. 9 respectively. Both of the figures show large scale oscillation in pressure as well as force history exerted on the entire bottom wall. This indicates that the compressible air may attribute to energy absorbing and releasing mechanism obtained at the impact moment. The linkage between the compressible air and pressure and force oscillation is further investigated in the following sections.

Another observation from the figures is that the results indeed converge when the time step becomes smaller than

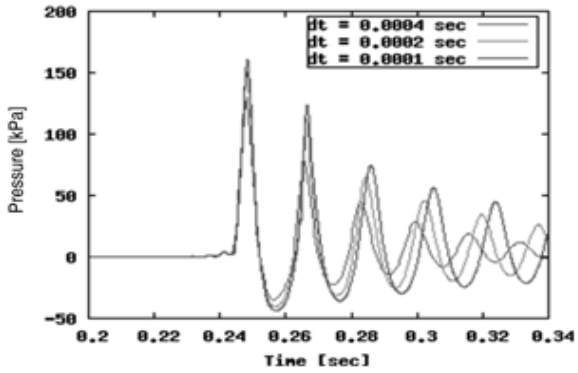

Fig. 8 Compressible air: pressure history measured at P0 (bottom center) with successively refined time steps. Oscillation in pressure history is evident. Grid-100 ×100 is used

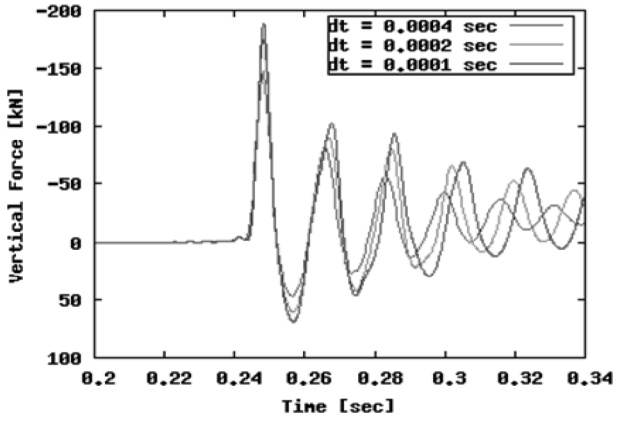

Fig. 9 Compressible air: vertical force exerted on the bottom wall with successively refined time steps. Negative force indicated downward force. Oscillation in force history is clearly resolved. Grid-100×100 is used

0.2millisecond for 100×100 grid. This study also shows that larger time step under-predicts the pressures and the vertical forces.

4.2.2 Incompressible Air

Now, the air is model as incompressible fluid. Similar to the compressible air case, we present time step refinement study for A1: 100×100 mesh. The pressure history is presented in Fig. 10 and the vertical force acting on the bottom surface is presented in Fig. 11.

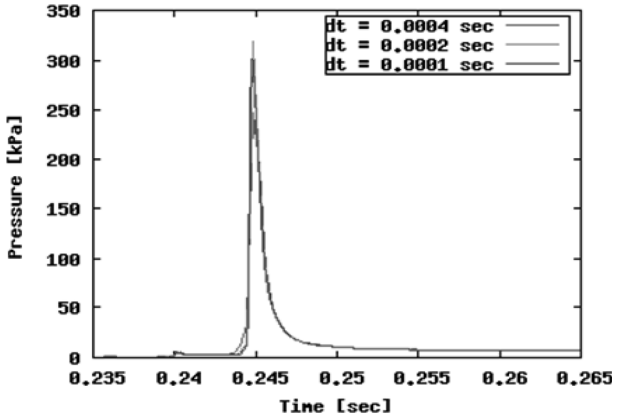

Fig. 10 Incompressible air: pressure history measured P0 (bottom center). No oscillation is observed. Grid-100×100 is used

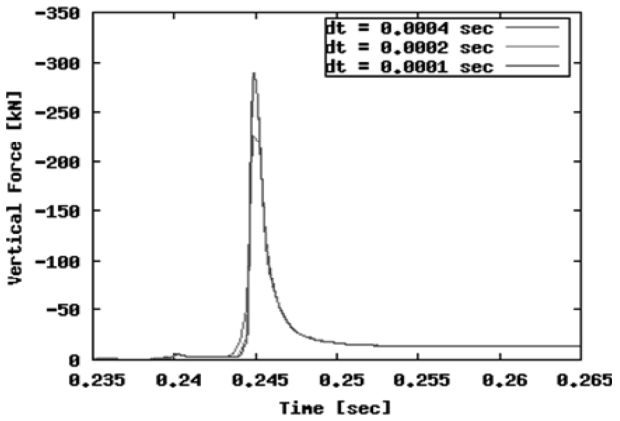

Fig. 11 Incompressible air: vertical force acting on the bottom wall. No oscillation is observed. Grid-100 ×100 is used

By the comparison of compressible air case(Fig. 8-9) and incompressible air case(Fig. 10-11), two important observations can be drawn. First, it is evident that air compressibility result in oscillations in the pressure as well as force acting on the bottom wall. Second, the incompressible air case shows much higher and sharp peak history than the compressible air case.

Based on this observation, it can be presumed that the oscillation is due to the air-cushion effect that originated from the entrapped air pocket between the solid surface and water. Such air pocket acts as a bumper to reduce the peak values in impact pressure and force as well as oscillation after the impact. Further evidence of our conjecture will be presented in the following sections.

4.2.3 Grid Refinement Study

It is well known that CFD results are sensitive to grid sizes. Three levels of successively refined meshes were used to check the convergence and sensitivity of the results depending on the mesh resolution. A1: 100×100 (i.e. single cell size 10mm ×10mm), A2: 200×200 (i.e. single cell size 5mm×5mm), A3: 400×400 (i.e. single cell size 2.5mm×2.5 mm).

As shown in Fig. 12-13, the peak values of the pressure

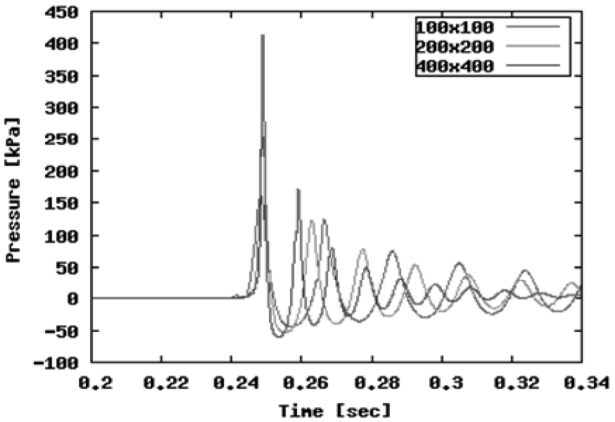

(a)

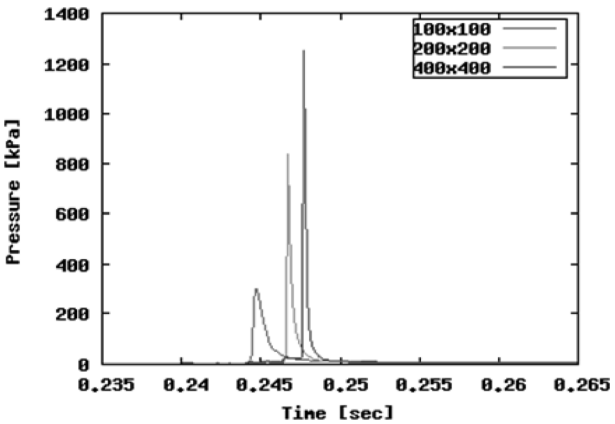

(b)

Fig. 12 Mesh convergence study: pressure history at bottom center obtained by successively refined meshes, (a) compressible air, (b) incompressible air. Compressible air cases show oscillation and lower peak values than incompressible air cases

and force highly depend on the mesh resolution. The results are extremely sensitive to the mesh resolution rather than the time step size.

Based on the observation of Fig. 12 and 13, there is no conclusive evidence of mesh convergence in peak pressure and force. In fact, the difference of peak value is rather becomes larger as mesh refines, which indicates typical divergence. This is clearly not a favorable indication for the validity of the result. Further investigation is necessary for the conclusive result about mesh refinement study.

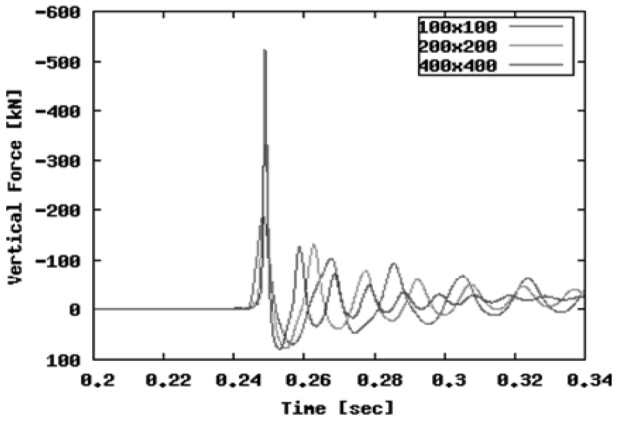

(a)

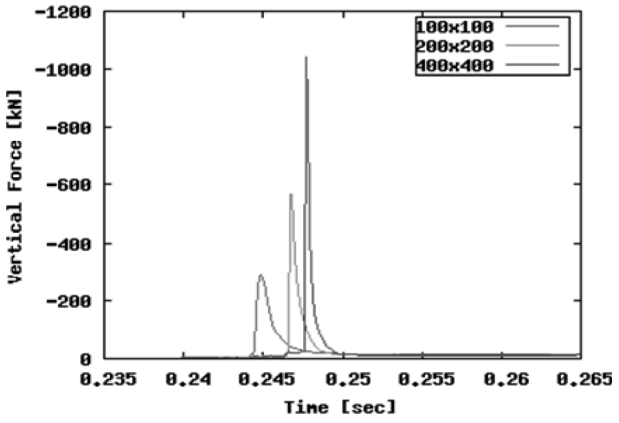

(b)

Fig. 13 Mesh convergence study: vertical force history obtained by successively refined meshes, (a) compressible air model, (b) incompressible air model. Compressible air cases show oscillation and lower peak values than incompressible air cases

However, in terms of the structural response and damage prediction, impulse exerted to the structure during certain period of time is more critical than a local pressure/force at a specific time moment. In that sense, we present the evolution of impulse during the water impact simulation. Fig. 15 shows that the impulse, $I(T)$, defined as

$$I(T)=\int_0^T f(t)dt$$

which is the integration of the force with respect to the simulation time. As shown in Fig. 14, superior mesh converge is obtained for impulse history, which is contrast to the pressure and force histories.

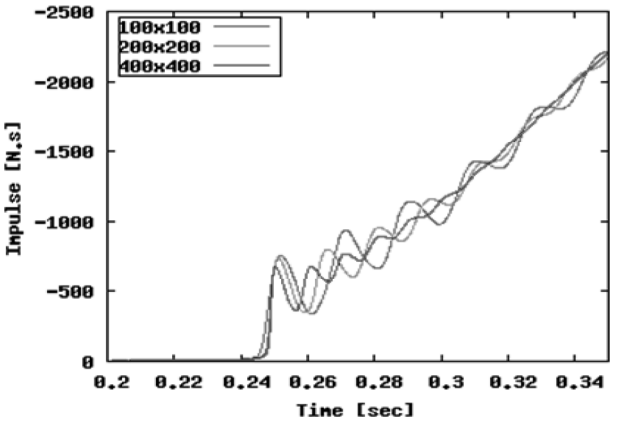

(a)

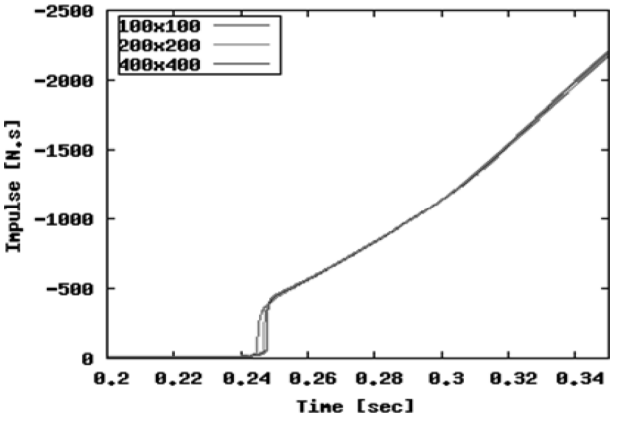

(b)

Fig. 14 Impulse predicted by using various grid sizes, (a) compressible air model, (b) incompressible air model. Oscillation is observed in the impulse history for compressible air case, while no such oscillation observed for incompressible air case

As shown in Fig. 14, the compressible air model reveals oscillatory evolution of impulse on the solid surface, whereas the incompressible air model shows monotonic increase of the impulse. Regardless of the model, both cases show convergence in impulse history as mesh refines.

4.2.4 Air Pockets and Pressure Oscillation

For the compressible air model, the fluid impact on the

tank wall results in the formation of a wide air layer as shown in Fig. 15. As the impact progresses, the air layer becomes large air pockets entrapped by water and bottom wall (Fig. 15a), then it collapses into many smaller air pockets (Fig. 15b).

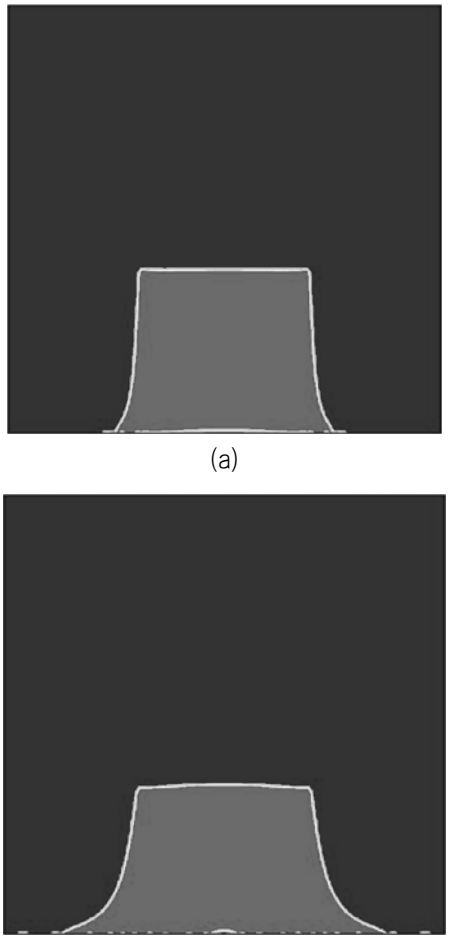

(a)

(b)

Fig. 15 Formation of air pocket on the bottom wall: (a) large air layer on the bottom, (b) air layer broken into smaller air pockets

The pressure oscillation can be explained by the results presented in Fig. 16. The water flow followed by the impact moment produces pressure oscillation in the bubble regions. When the air pockets are compressed by surround fluid motion, the air pressure exceeds the surrounding water pressure, as shown in Fig. 16a. At this time, the air pockets size reduces due to air compression. Later, the air pocket with higher pressure redirects the water flow away from the air bubble, and this process results in a lower pressure in the air than in the surrounding fluid, as shown in Fig. 16b. At this time, the air pocket expands. Throughout this process, the air pocket acts as a spring that absorbs the kinetic energy from the impact moment and results in oscillations in pressure and force history. This oscillation eventually decays due to viscous diffusion of the governing equations.

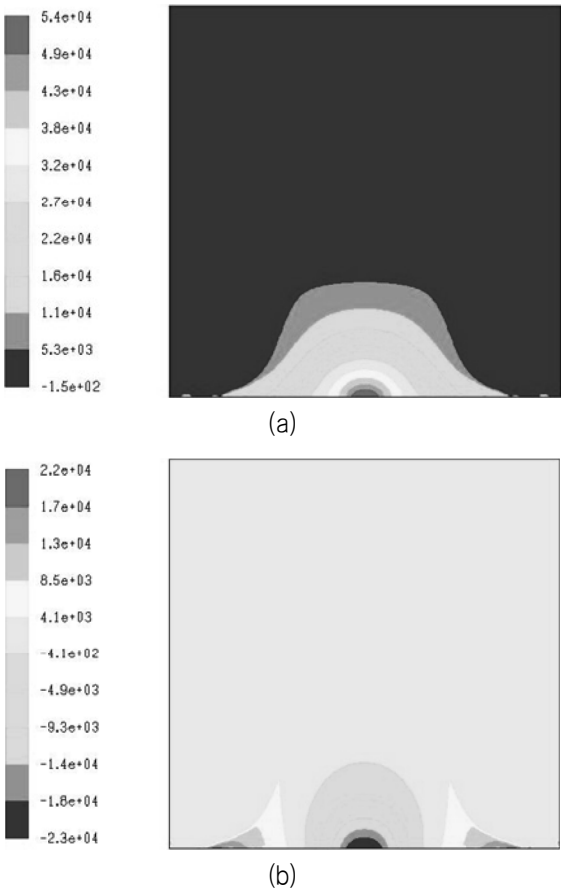

(a)

(b)

Fig. 16 Pressure oscillation in the air pocket. (a) bubble compression(positive pressure), t=0.276s, (b) bubble expansion(negative pressure), t=0.282s

4.2.5 Scale Effect

In order to investigate the effect of the domain size to the results, a series of simulation was carried out with various domain sizes: 1m×1m, 2m×2m, 4m×4m, 8m×8m, 16m×16m. In order to quantify the air compressibility effect on this water drop example, we propose air compressibility indicator based on the normalized impulse difference between compressible and incompressible air simulations as follows

$$\gamma = \left| \frac{I_i - I_c}{I_i} \right|$$

Here, I_i is the impulse obtained from the incompressible air simulation and I_c is the impulse from the compressible air model defined as follows

$$I_i = \int_0^T f_i(t)dt,\ \ I_c = \int_0^T f_c(t)dt$$

where f_i and f_c are the force history for compressible and incompressible air models respectively and T is the integration interval defined as $T = \frac{\pi}{2}\sqrt{\frac{L}{g}}$.

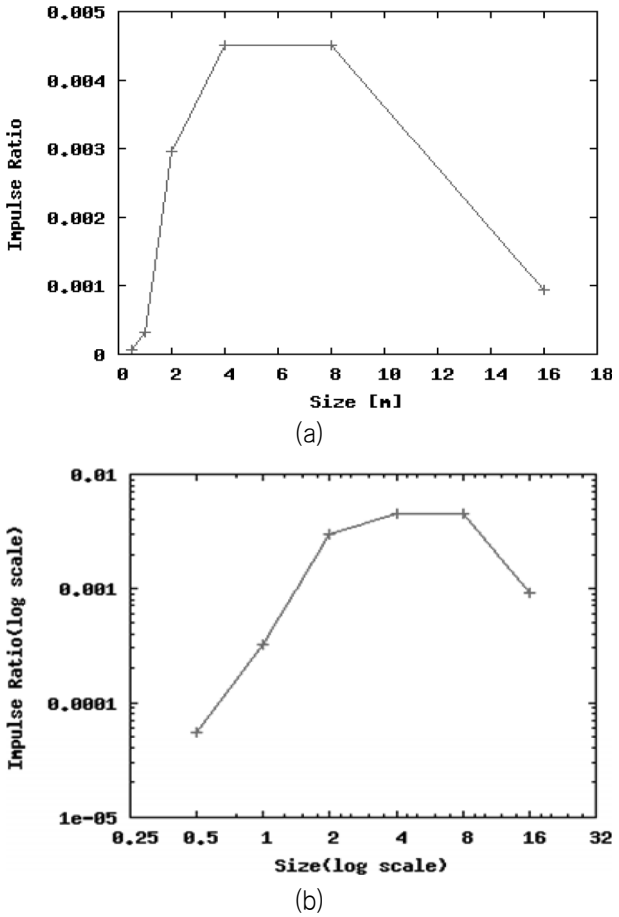

Fig. 17 Impulse difference ratio, γ, between the compressible and incompressible air simulations. (a) linear scale, (b) log scale

Fig. 17 shows the trend of impulse ratio value with respects to domain size. The impulse ratio, γ, which is an indicator of air compressibility effect has its maximum for the scale of meters, and diminishes either for the smaller size (length scale: $L<1m$) or for the larger size (length scale: $L<10m$). In other words, the effects of air compressibility play a more important role when the domain size is in the order of meters, whereas less significant for the domain very small or very large.

This result seems to follows our intuition. For very small scale, the fluid inertia is not big enough for the air to feel compressibility effect. For very large scale, inertia is too big, so the air compressibility plays minor role for the total impulse. The air compressibility seems to be the maximum when the length is meter scale, where usual laboratory experiment is being conducted. This result implies that air compressibility has to be considered more carefully for laboratory scale water impact experiments.

5. Water Entry Problem

5.1 Problem Definition

In order to strengthen the conclusion the effect of air compressibility, we propose another, yet more practical case, which is a rigid body water entry problem. The constant velocity water entry model in this study is presented as shown in Fig. 18. In this model, the tank size is L=1 m, H=1 m and a rectangular rigid body with 0.1 m wide, 0.1 m height. The rectangular body is set to move downward from 0.1 m above the calm water free surface with constant speed of 1.4 m/s, which is the impact velocity in free-fall condition. For impact pressure measurement, a sensor point P0 is defined at the center on the bottom of the moving body. As shown in figure 18, the boundary conditions are all set as no-slip wall conditions except for the tank top, which is set as pressure outlet. The pressure outlet boundary condition maintains a zero gauge pressure at the defined boundary, which is desired for the tank top.

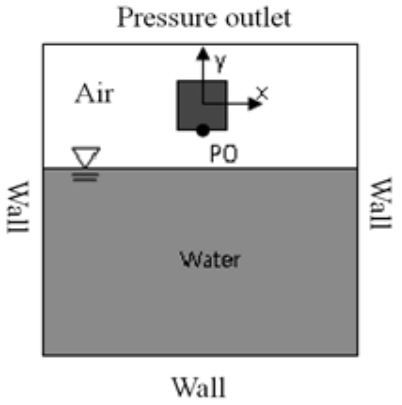

Fig. 18 General layout of the water entry problem and boundary conditions

5.2 Simulation Results

5.2.1 Compressible Air

Fig. 19 shows the pressure time history at the point P0 for the grid size 200x200. The time step convergence was studied

with various time step sizes. It was found that the larger time step case under-predicts the initial peak pressure. As the time step refines the results converges, especially if the step size is smaller than 0.2millisecond.

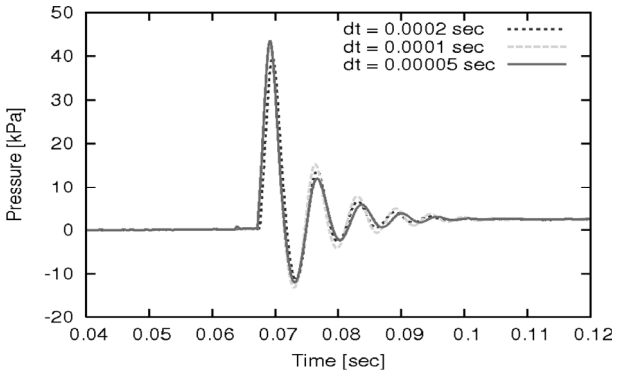

Fig. 19 Pressure time history at P0, compressible air

In term of structural response and damage prediction, impulse exerted to the structure during certain period of time is more important rather than a local pressure at a specific time moment(Faltinsen 1990, Shin et al. 2010). In those sense, we present the evolution of impulse during the water impact simulation. Fig. 20 shows that the impulse, which is defined as the integral of the lift force with respect to time, is converged when the grid size is refined.

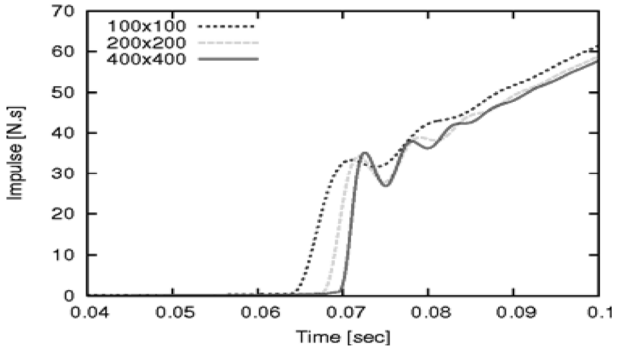

Fig. 20 Impulse convergence study, compressible air

Furthermore, the author like to emphasize that the oscillations in the pressure as shown in Fig. 19 is also observed in the experimental study by Shin et al.(2010) in a similar manner, which strengthens the validity of current simulation of water impact problem.

5.2.2 Incompressible Air

Similar to the compressible air case, we present time step refinement study for the grid size 200x200. The pressure time history is presented in Fig. 21.

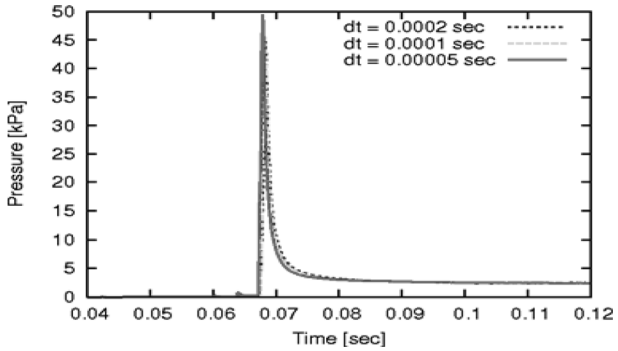

Fig. 21 Pressure time history at P0, incompressible air

By the comparison of compressible air simulation (Fig. 19), it is evident that air compressibility result in oscillations in the impact pressure history. This oscillation is presumed to be due to the air-cushion effect that originated from the entrapped air pocket between the solid surface and water.

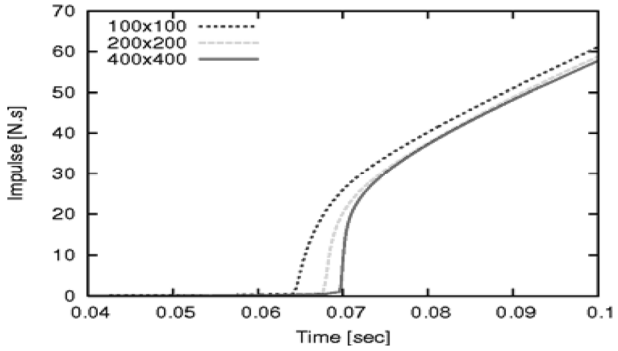

Fig. 22 Impulse convergence study, incompressible air

Fig. 22 shows the impulse convergence study of the incompressible air case. Three grid sizes are employed: 100×100, 200×200, 400×400. The impulse time history of the incompressible air model shows monotonic increase of the impulse value, whereas the compressible air model reveals oscillatory evolution of impulse on the body surface (Fig. 20). This further strengthens our finding that the compressible air model correctly predicts the air-cushion effect at the impact moment.

6. Conclusion

Air compressibility effect in water impact problem is investigated by CFD simulations. In order to investigate the air compressibility effect, the air is modeled as compressible ideal gas as well as incompressible fluid. For both cases, the water is modeled as incompressible fluid. By the comparison of impact load response, compressible air model showed that oscillatory behavior in pressure and force histories acting on

the solid surface. Such oscillation decays as time goes due to the viscous dissipation. On contrary, incompressible air model showed no such oscillatory behavior in neither pressure nor force responses. Incompressible air model showed only a single sharp peak in pressure and force response followed by the impact moment. The current CFD simulation also resolved that the oscillation is due to the air pockets generated on the solid surface where the pressure oscillates. Mesh refinement study showed that the impulse exerted during the impact process is convergent, while further study is to be carried about the convergence of the peak pressure and forces. Lastly, the scale effect study showed that air compressibility, represented by the impulse difference, is biggest for the scale of meters, which requests further investigation of air compressibility also in laboratory experiments

Acknowledgement

This work was supported by the 2009 Research Fund of University of Ulsan.

References

Faltinsen, O.M., 1990, *Sea loads on ships and offshore structures*, Cambridge University Press.

Fluent, 2008, Ver. 6.3., User Manual.

Godderidge, B. Tunock, S. Earl C. & Tan M., 2009. The effect of fluid compressibility on the simulation of sloshing impacts. *Ocean Engineering,* 36, pp. 578-587.

Howison, S.D. Ockendon, J.R. & Wilson, S.K. 1991. Incompressible water-entry problems at small dead-rise angles. *Journal of Fluid Mechanics,* 222, pp. 215-230.

Kang, C.G. & Troesch, A. W., 1990. Prediction of Hydrodynamic Impact Loads on Three-Dimensional Bodies. *Journal of the Society of Naval Architects of Korea,* 27(3), pp. 73-88.

Kleefsman, K.M.T. Fekken, G. Veldman, A.E.P. Buchner, B. & Iwanowski, B. 2005. A Volume-of-Fluid based simulation method for wave impact problems. *Journal of Computational Physics,* 206, pp. 363-393.

Korobkin, A.A. & Iafrati, A. 2005. Hydrodynamic loads during initial stage of floating body impact. *Journal of Fluids and Structures,* 21, pp. 413-427.

Kwon, S.H. Chung, J.Y. Kwak, D.W. Lee, S.H. & Choi, Y.M. 2010. A Note on Slamming. *The 6th National Congress on Fluids Engineering,* Busan, Republic of Korea, 18-20 August 2010, pp. 779-780.

Lee, B.Y. Park, J.C. Jung, S.J. Ryu, M.C. & Ki, Y.S., 2008. Numerical Simulation for Fluid Impact Load by Flat Plate with Incident Angles. *Journal of the Society of Naval Architects of Korea,* 45(1), pp. 1-9.

Nho, I. S. Lee J. M. & Yeom, C. W., 2010. A Fundamental Study for Time History Modeling of Fluid Impact Pressure. *Journal of the Society of Naval Architects of Korea,* 47(2), pp. 242-247,

Scardovelli, R. & Zaleski, S., 1999. Direct numerical simulation of free-surface and interfacial flow, *Annual Review of Fluid Mechanics,* 31, pp. 567-603.

Shin, H. Kim, S.-C. & Cho, S.-R., 2010. Experimental Investigations on Slamming Impacts by Drop Tests. *Journal of the Society of Naval Architects of Korea,* 47(3), pp. 410-420.

Sun, H. & Faltinsen, O.M., 2006. Water impact of horizontal circular cylinders and cylindrical shells. *Applied Ocean Research,* 28, pp. 299-311.

Wu, G.X., 1998. Hydrodynamic force on a rigid body during impact with liquid. *Journal of Fluids and Structures,* 12, pp. 549-559.

Wu, G. X. Sun, H. & He, Y. S., 2004. Numerical simulation and experimental study of water entry of a wedge in free fall motion. *Journal of Fluid and Structures,* 19, pp. 277-289.

Yoon, B.S., 1991. Lagrangian Finite Element Analysis of Water Impact Problem. *Journal of the Society of Naval Architects of Korea,* 28(1), pp. 60-68.

Yum, D.J. & Yoon, B.S., 2008. Numerical Simulation of Slamming Phenomena for 2-D Wedges. *Journal of the Society of Naval Architects of Korea,* 45(5), pp. 477-486.

Zhang, Y. Zou, Q. & Greaves, D., 2010. A level set immersed boundary method for water entry and exit. *Communication in Computational Physics,* 8, pp. 265-288.

Zhao, R. & Faltinsen, O., 1993. Water Entry of Two-dimensional Bodies. *Journal of Fluid Mechanics,* 246, pp. 593-612.

찬 후 피

안 형 택